ATLAS NOTE

ATLAS-CONF-2015-062

14th December 2015

Search for squarks and gluinos in final states with jets and missing transverse momentum at $\sqrt{s}$ =13 TeV with the ATLAS detector

The ATLAS Collaboration

Abstract

A search for squarks and gluinos in final states containing jets, missing transverse momentum and no electrons or muons is presented. The data were recorded in 2015 by the ATLAS experiment in $\sqrt{s}$ = 13 TeV proton-proton collisions at the Large Hadron Collider. No excess above the Standard Model background expectation was observed in 3.2 fb^{-1} of analysed data. Results are interpreted within simplified models assuming that R-parity is conserved and with a neutralino as the lightest supersymmetric particle. An exclusion limit at the 95% confidence level on the mass of the gluino is set at 1520 GeV for a simplified model incorporating only a gluino octet and the lightest neutralino, assuming the lightest neutralino is massless. For a simplified model involving the strong production of mass-degenerate first- and second-generation squarks, squark masses below 980 GeV are excluded for a massless lightest neutralino. These limits extend the region of supersymmetric parameter space excluded by previous measurements with the ATLAS detector.

ATLAS-CONF-2015-062
15 December 2015

1 Introduction

Supersymmetry (SUSY) [1–6] is a generalization of space-time symmetries that predicts new bosonic partners for the fermions and new fermionic partners for the bosons of the Standard Model (SM). If R-parity is conserved [7], SUSY particles (called sparticles) are produced in pairs and the lightest supersymmetric particle (LSP) is stable. The scalar partners of the left- and right-handed quarks, the squarks $\tilde{q}_{\mathrm{L}}$ and $\tilde{q}_{\mathrm{R}}$, mix to form two mass eigenstates $\tilde{q}_1$ and $\tilde{q}_2$ ordered by increasing mass. Squarks and the fermionic partners of the gluons, the gluinos ($\tilde{g}$), could be produced in strong interaction processes at the Large Hadron Collider (LHC) [8] and decay via cascades ending with the stable LSP which escapes the detector unseen producing substantial missing transverse momentum ($\boldsymbol{E}_{\mathrm{T}}^{\mathrm{miss}}$). The mass eigenstates formed from the linear superpositions of the superpartners of the charged and neutral electroweak and Higgs bosons are respectively the charginos ($\tilde{\chi}^{\pm}$) and neutralinos ($\tilde{\chi}^{0}$).

The production of gluinos and squarks is the primary target for early supersymmetry searches in proton–proton (pp) collisions at a centre-of-mass energy of 13 TeV at the LHC because of their large expected cross-sections. This document presents a search for these particles in final states containing only jets and large missing transverse momentum. Interest in this final state is motivated by the large number of R-parity-conserving [9, 10] models in which squarks (including anti-squarks) and gluinos can be produced in pairs ($\tilde{g}\tilde{g}$, $\tilde{q}\tilde{q}$, $\tilde{q}\tilde{g}$) and can decay through $\tilde{q} \to q\tilde{\chi}_1^0$ and $\tilde{g} \to q\bar{q}\tilde{\chi}_1^0$ to neutralinos, $\tilde{\chi}_1^0$, assumed to be the LSP. Additional decay modes can include the production of charginos via $\tilde{q} \to q\tilde{\chi}^{\pm}$ (where $\tilde{q}$ and q are of different flavour) and $\tilde{g} \to q\bar{q}\tilde{\chi}^{\pm}$. Subsequent chargino decay to $W^{\pm}\tilde{\chi}_1^0$ can lead to final states with even larger multiplicities of jets. The analysis presented here adopts the same analysis strategy as the previous search designed for the analysis of the 7 TeV and 8 TeV data collected during Run 1 of the LHC, described in Refs. [11–14] and extended with new SUSY model interpretations in Ref. [15]. Further results of relevance to these models were published by the CMS collaboration [16–21].

In this search, events with reconstructed electrons or muons are vetoed to reduce the background from events with hard neutrinos and to avoid the overlap with a related ATLAS search [22]. The search strategy is optimised in the $(m_{\tilde{g}}, m_{\tilde{\chi}_1^0})$ and $(m_{\tilde{q}}, m_{\tilde{\chi}_1^0})$ planes, (where $m_{\tilde{g}}$, $m_{\tilde{q}}$ and $m_{\tilde{\chi}_1^0}$ are the gluino, squark and the LSP masses respectively) for simplified models [23–25] in which all other supersymmetric particles are assigned masses beyond the reach of the LHC. Although interpreted in terms of SUSY models, this analysis could also constrain any model of new physics that predicts the production of jets in association with missing transverse momentum.

2 The ATLAS detector and data samples

The ATLAS detector [26] is a multi-purpose particle physics detector with a forward-backward symmetric cylindrical geometry and nearly 4π coverage in solid angle.[1] The inner tracking detector (ID) consists of pixel and silicon microstrip detectors covering the pseudorapidity region $|\eta| < 2.5$, surrounded by a

[1] ATLAS uses a right-handed coordinate system with its origin at the nominal interaction point in the centre of the detector. The positive x-axis is defined by the direction from the interaction point to the centre of the LHC ring, with the positive y-axis pointing upwards, while the beam direction defines the z-axis. Cylindrical coordinates (r, ϕ) are used in the transverse plane, ϕ being the azimuthal angle around the z-axis. The pseudorapidity η is defined in terms of the polar angle θ by $\eta = -\ln\tan(\theta/2)$ and the rapidity is defined as $y = 1/2\ln[(E + p_z)/(E - p_z)]$ where E is the energy and p_z the longitudinal momentum of the object of interest. The transverse momentum p_{T}, the transverse energy E_{T} and the missing transverse momentum $E_{\mathrm{T}}^{\mathrm{miss}}$ are defined in the $x - y$ plane unless stated otherwise.

transition radiation tracker which enhances electron identification in the region $|\eta| < 2.0$. The innermost pixel layer, the insertable B-layer [27], was added between Run 1 and Run 2 of the LHC, at a radius of 33 mm around a new, thinner, beam pipe. The ID is surrounded by a thin superconducting solenoid providing an axial 2 T magnetic field and by a fine-granularity lead/liquid-argon (LAr) electromagnetic calorimeter covering $|\eta| < 3.2$. A steel/scintillator-tile calorimeter provides hadronic coverage in the central pseudorapidity range ($|\eta| < 1.7$). The endcap and forward regions ($1.5 < |\eta| < 4.9$) of the hadronic calorimeter are made of LAr active layers with either copper or tungsten as the absorber material. An extensive muon spectrometer with an air-core toroid magnet system surrounds the calorimeters. Three layers of high-precision tracking chambers provide coverage in the range $|\eta| < 2.7$, while dedicated fast chambers allow triggering in the region $|\eta| < 2.4$.

The ATLAS trigger system [28] consists of two levels; the first level is a hardware-based system, while the second is a software-based system called the High Level Trigger. The events used in this search were selected using a trigger logic that accepts events with missing transverse momentum, calibrated to the electromagnetic scale, above 70 GeV. The trigger is 100% efficient for the event selections considered in this analysis. Auxiliary data samples used to estimate the yields of background events were selected using triggers requiring a single isolated electron ($p_{\mathrm{T}} > 24$ GeV), muon ($p_{\mathrm{T}} > 20$ GeV) or photon ($p_{\mathrm{T}} > 120$ GeV). To recover possible efficiency losses at high momenta, additional single electron and muon triggers that do not require any isolation were included with thresholds of $p_{\mathrm{T}} > 60$ GeV and 50 GeV, for electron and muon respectively.

The dataset used in this analysis was collected in 2015 with the LHC colliding 6.5 TeV proton beams with 25 ns bunch spacing. The peak delivered instantaneous luminosity was $L = 5.2 \times 10^{33}\mathrm{cm}^{-2}\mathrm{s}^{-1}$ and the average number of expected interactions per proton-proton bunch crossing ranged from approximately 5 to 25, with a mean of 14. Application of beam, detector and data-quality requirements resulted in a total integrated luminosity of 3.2 fb^{-1}. The uncertainty on the integrated luminosity is ±5%. It is derived, following a methodology similar to that detailed in Ref. [29], from a preliminary calibration of the luminosity scale using a pair of x-y beam-separation scans performed in August 2015.

3 Monte Carlo simulated samples

Monte Carlo (MC) data samples are used to develop the analysis, optimise the selections, estimate backgrounds and assess the sensitivity to specific SUSY signal models.

SUSY signals are described by simplified models. They are defined by an effective Lagrangian describing the interactions of a small number of new particles, typically assuming one production process and one decay channel with a 100% branching fraction. Signal samples used to describe squark- and gluino-pair production, followed by the direct[2] decays of squarks ($\tilde{q} \to q\tilde{\chi}_1^0$) and direct ($\tilde{g} \to q\bar{q}\tilde{\chi}_1^0$) or one-step[3] ($\tilde{g} \to q\bar{q}'W\tilde{\chi}_1^0$) decays of gluinos as shown in Figure 1, are generated with up to two extra partons in the matrix element using MADGRAPH 5.2.1.2 [30] interfaced to PYTHIA 8.186 [31]. The CKKW-L merging scheme [32] is applied with a scale parameter that is set to a quarter of the mass of the gluino for $\tilde{g}\tilde{g}$ production or of the squark for $\tilde{q}\tilde{q}$ production. The ATLAS underlying-event tune A14 [33] is used together with the NNPDF2.3LO [34] parton distribution function (PDF) set. The EVTGEN v1.2.0 program [35] is used to describe the properties of the bottom and charm hadron decays in the signal samples and the

[2] Direct decays are those where the considered SUSY particles decay directly into SM particles and the LSP.
[3] One-step decays refer to the cases where the decays occur via one intermediate on-shell SUSY particle.

background samples except those produced with SHERPA [36]. The signal cross-sections are calculated at next-to-leading order (NLO) in the strong coupling constant, adding the resummation of soft gluon emission at next-to-leading-logarithmic accuracy (NLO+NLL) [37–41]. The nominal cross-section is taken from an envelope of cross-section predictions using different PDF sets and factorisation and renormalisation scales, as described in Ref. [42]. Only light-flavour quarks (u, d, s, c) are considered. Cross-sections are evaluated assuming masses of 450 TeV for the light-flavour squarks or gluinos in cases of gluino- and squark-pair productions, respectively. The free parameters in these models are $m_{\tilde{q}}$ or $m_{\tilde{g}}$, and $m_{\tilde{\chi}_1^0}$.

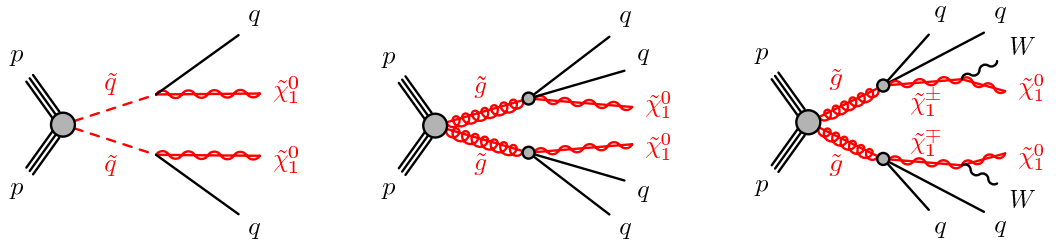

Figure 1: The decay topologies of (a) squark-pair production and (b, c) gluino-pair production, in the simplified models with direct decays of squarks and direct or one-step decays of gluinos.

The summary of the SM background processes together with the MC generators, cross-section calculation orders in α_s, PDFs, parton shower and tunes used are listed in Table 1.

Table 1: The Standard Model background Monte Carlo simulation samples used in this paper. The generators, the order in α_s of cross-section calculations used for yield normalization (leading order (LO), next-to-leading order (NLO), next-to-next-to-leading order (NNLO), next-to-next-to-leading logarithm (NNLL)), PDF sets, parton showers, and tunes used for the underlying event are shown.

Physics process	Generator	Cross-section normalisation	PDF set	Parton shower	Tune
$W(\to \ell\nu)$ + jets	SHERPA 2.1.1	NNLO	CT10	SHERPA	SHERPA default
$Z/\gamma^*(\to \ell\bar{\ell})$ + jets	SHERPA 2.1.1	NNLO	CT10	SHERPA	SHERPA default
γ + jets	SHERPA 2.1.1	LO	CT10	SHERPA	SHERPA default
$t\bar{t}$	POWHEG-BOX v2	NNLO+NNLL	CT10	PYTHIA 6.428	PERUGIA2012
Single top (t-channel)	POWHEG-BOX v1	NLO	CT10f4	PYTHIA 6.428	PERUGIA2012
Single top (s- and Wt-channel)	POWHEG-BOX v2	NLO	CT10	PYTHIA 6.428	PERUGIA2012
$t\bar{t}+W/Z/WW$	MADGRAPH 5.2.2.2	NLO	NNPDF2.3LO	PYTHIA 8.186	A14
WW, WZ, ZZ	SHERPA 2.1.1	NLO	CT10	SHERPA	SHERPA default
Multi-jet	PYTHIA 8.186	LO	NNPDF2.3LO	PYTHIA 8.186	A14

The production of γ, W or Z bosons in association with jets is simulated using the SHERPA 2.1.1 generator. For W or Z bosons, the matrix elements are calculated for up to two partons at NLO and up to additional two partons at leading order (LO) using the COMIX [43] and OPENLOOPS [44] matrix element generators, and merged with the SHERPA parton shower [45] using the ME+PS@NLO prescription [46]. Events containing a photon in association with jets are generated requiring a photon transverse momentum above 35 GeV. For these events, matrix elements are calculated at LO with up to three or four partons depending on the p_T of the photon, and merged with SHERPA parton shower using the ME+PS@LO prescription [47].

In both cases (W/Z + jets or γ + jets production), the CT10 PDF set [48] is used in conjunction with dedicated parton shower tuning developed by the Sherpa authors. The W/Z + jets events are normalized to their NNLO cross-sections [49]. For the γ+jets process the LO cross-section, taken directly from the Sherpa MC generator, is multiplied by a correction factor as described in Section 7.

For the generation of $t\bar{t}$ and single top processes in the Wt and s-channel the Powheg-Box v2 [50] generator is used with the CT10 PDF set. The electroweak t-channel single top events are generated using the Powheg-Box v1 generator. This generator uses the four-flavour scheme for the NLO matrix elements calculations together with the fixed four-flavour PDF set CT10f4 [48]. For this process, the top quarks are decayed using MadSpin [51] preserving all spin correlations, while for all processes the parton shower, fragmentation and the underlying event are generated using Pythia 6.428 [52] with the CTEQ6L1 [53] PDF set and the corresponding Perugia 2012 tune (P2012) [54]. The top quark mass is set to 172.5 GeV. The $t\bar{t}$ (single top) events are normalized to the NNLO+NNLL [55, 56] (NLO) cross-sections.

For the generation of $t\bar{t}+W/Z/WW$ processes Madgraph 5.2.2.2 [30] generator at LO interfaced to the Pythia 8.186 parton shower model is used, with up to two ($t\bar{t}+W$), one ($t\bar{t}+Z$) or no ($t\bar{t}+WW$) extra partons included in the matrix element. The ATLAS underlying-event tune A14 is used together with the NNPDF2.3LO PDF set. The events are normalised to their respective NLO cross-sections [57, 58].

Diboson processes (WW, WZ, ZZ) are simulated using the Sherpa 2.1.1 generator. For processes with four charged leptons (4ℓ), three charged leptons and a neutrino (3ℓ+1ν) or two charged leptons and two neutrinos (2ℓ+2ν), matrix elements contain all diagrams with four electroweak vertices, and are calculated for up to one (4ℓ, 2ℓ+2ν) or no partons (3ℓ+1ν) at NLO and up to three partons at LO using the Comix and OpenLoops matrix element generators, and merged with the Sherpa parton shower using the ME+PS@NLO prescription. For processes in which one of the bosons decays hadronically and the other leptonically, matrix elements are calculated for up to one (ZZ) or no (WW, WZ) additional partons at NLO and for up to three additional partons at LO using the Comix and OpenLoops matrix element generators, and merged with the Sherpa parton shower using the ME+PS@NLO prescription. In all cases, the CT10 PDF set is used in conjunction with a dedicated parton shower tuning developed by the Sherpa authors. The generator cross-sections are used in this case.

The multi-jet background is generated with Pythia 8.186 using the A14 underlying event tune and the NNPDF2.3LO parton distribution functions.

All Standard Model background samples are passed through the full ATLAS detector simulation [59] based on Geant4 [60]. Signal samples are passed through the fast simulation which uses a parameterization of the performance of the ATLAS electromagnetic and hadronic calorimeters [61] and Geant4 elsewhere.

4 Object reconstruction and identification

The reconstructed primary vertex of the event is required to be consistent with the beamspot envelope and to have at least five associated tracks with $p_{\mathrm{T}} > 400$ MeV. When more than one such vertex is found, the vertex with the largest $\sum p_{\mathrm{T}}^2$ of the associated tracks is chosen.

Jet candidates are reconstructed using the anti-k_t jet clustering algorithm [62, 63] with a radius parameter of 0.4. The inputs to this algorithm are topological clusters [64, 65] of calorimeter cells seeded by those with energy significantly above the measured noise (topoclusters). The jets are corrected for energy

from pile-up (multiple pp interactions in the same or neighbouring bunch-crossings) using the method suggested in Ref. [66]: a contribution equal to the product of the jet area and the median energy density of the event is subtracted from the jet energy [67]. Further corrections, referred to as the jet energy scale (JES) corrections, are derived from MC simulation and data and used to calibrate on average the energies of jets to the scale of their constituent particles [68]. Only jet candidates with $p_{\mathrm{T}} > 20$ GeV and $|\eta| < 2.8$ after all corrections are retained. A boosted-decision-tree-based algorithm 'MV2c20' is used to identify jets containing a b-hadron (b-jets), with an operating point corresponding to an efficiency of 77% in simulated $t\bar{t}$ events, along with a rejection factor of 140 for gluon and light-quark jets and of 4.5 for charm jets [69, 70]. Candidate b-tagged jets must be within $|\eta| < 2.5$. Events with jets from detector noise and non-collision background are rejected if they fail to satisfy the "LooseBad" quality criteria, or if at least one of the two leading jets in event fails to satisfy the "TightBad" quality criteria described in Ref. [71] and has $p_{\mathrm{T}} > 100$ GeV. These selections suppress less then 1% of the events used in the search.

Two different classes of reconstructed leptons (electrons or muons) are used in this analysis. When selecting samples used for the search, events containing a 'baseline' electron or muon are rejected. The selections applied to baseline leptons are designed to maximise the efficiency with which W+jets and top quark background events are rejected. When selecting 'control region' samples for the purpose of estimating residual W+jets and top quark backgrounds, additional requirements are applied to leptons to ensure greater purity. These leptons are referred to as 'high-purity' leptons below and form a subset of the baseline leptons.

Baseline electron candidates are required to have $p_{\mathrm{T}} > 10$ GeV and $|\eta| < 2.47$, and to satisfy 'loose' likelihood-based identification criteria described in Ref. [72]. High-purity electron candidates additionally must have $p_{\mathrm{T}} > 25$ GeV, satisfy tighter selection criteria, have the significance of the transverse impact parameter with respect to the primary vertex, $|d_0^{PV}|/\sigma(d_0^{PV}) < 5$, and the longitudinal impact parameter with respect to the primary vertex $|z_0 \cdot \sin(\theta)| < 0.5$ mm, and to be isolated from nearby energetic particles.

Baseline muon candidates are formed by combining information from the muon spectrometer and inner tracking detectors as described in Ref. [73] and are required to have $p_{\mathrm{T}} > 10$ GeV and $|\eta| < 2.5$. High-purity muon candidates must additionally have $p_{\mathrm{T}} > 25$ GeV, $|\eta| < 2.4$, the significance of the transverse impact parameter with respect to the primary vertex, $|d_0^{PV}|/\sigma(d_0^{PV}) < 3$, and longitudinal impact parameter with respect to the primary vertex $|z_0 \cdot \sin(\theta)| < 0.5$ mm, and to be isolated from nearby energetic particles.

After the selections described above, ambiguities between candidate jets with $|\eta| < 2.8$ and leptons are resolved as follows. First, any such jet candidate lying within a distance $\Delta R \equiv \sqrt{(\Delta y)^2 + (\Delta\phi)^2} = 0.2$ of a baseline electron is discarded; then any baseline lepton candidate remaining within a distance $\Delta R = 0.4$ of any surviving jet candidate is discarded, except for the case when the lepton is a muon and the number of tracks associated to the jet is less than three.

Additional ambiguities between electrons and muons in a jet, originating from the decays of hadrons, are applied to avoid double counting and/or remove non-isolated leptons: the electron is discarded if a baseline electron and a baseline muon share the same ID track. If two baseline electrons are within $\Delta R < 0.05$, the electron with the lowest p_{T} is discarded.

The measurement of the missing transverse momentum two-dimensional vector $\boldsymbol{E}_{\mathrm{T}}^{\mathrm{miss}}$ (and its magnitude $E_{\mathrm{T}}^{\mathrm{miss}}$) is based on the calibrated transverse momenta of all electron, muon, photon and jet candidates and and all tracks originating from the primary vertex and not associated with such objects [74].

Reconstructed photons, although not used in the main signal event selection, are used to constrain the Z+jets background. Photon candidates are required to possess $p_{\mathrm{T}} > 130$ GeV and $|\eta| < 2.37$, to satisfy photon shower shape and electron rejection criteria [75], and to be isolated. Ambiguities between candidate jets and photons (when used in the event selection) are resolved by discarding any jet candidates lying within $\Delta R = 0.2$ of a photon candidate. The transverse momenta of the resulting reconstructed photons are taken into account when calculating $\boldsymbol{E}_{\mathrm{T}}^{\mathrm{miss}}$. Additional ambiguities between electrons or muons and photons are applied such that the photon is discarded if it is within $\Delta R < 0.4$ of an electron or muon.

Corrections derived from data control samples are applied to account for differences between data and simulation for the lepton trigger and reconstruction efficiencies, the lepton momentum/energy scale and resolution, and for the efficiency and mis-tag rate of the b-tagging algorithm.

5 Analysis strategy and fit description

To search for a possible signal, selections are defined to enhance the signal with respect to the SM background. These signal region (SR) selections are optimized to maximize the expected significance for each model considered using MC simulation for the signal and the SM backgrounds. To estimate the SM backgrounds in a consistent and robust fashion, corresponding control regions (CRs) are defined for each of the signal regions. They are chosen to be non-overlapping with the SR selections in order to provide independent data samples enriched in particular background sources, and are used to normalize the background MC simulation. The CR selections are optimized to have negligible SUSY signal contamination for the models near the previously excluded boundary [14], while minimizing as much as possible the systematic uncertainties arising from the extrapolation of the CR event yields to the expectations in the SR. Cross-checks of the background estimates are performed using several validation regions (VRs) selected with requirements such that these regions do not overlap with the CR and SR selections, again with a low expected signal contamination.

To extract the final results, three different classes of likelihood fit are employed [76]. A background-only fit is used to determine the compatibility of the observed event yield in each SR with the corresponding SM background expectation. The fit is performed using as constraints only the observed event yields from the CRs associated with the SR, but not the SR itself. It is assumed that signal events from physics beyond the Standard Model (BSM) do not contribute to these yields. The inputs to the fit for each of the SRs are the numbers of events observed in each of the CRs, and the corresponding numbers of events expected from simulation. The scale factors ($\mu_{W+\mathrm{jets}}, \mu_{Z+\mathrm{jets}}, \mu_{\mathrm{Top}}, \mu_{\mathrm{Multi-jet}}$) are fitted in each CR attached to a SR. The extrapolation from CR to SR is based on the yields predicted by simulation, corrected by the scale factors derived from the fit, and on which systematic uncertainties are evaluated by varying the corresponding MC inputs. The background-only fit is also used to estimate the background event yields in the VRs.

If no excess is observed, a model-independent fit is used to set upper limits on the number of BSM signal events in each SR. This fit proceeds in the same way as the background-only fit, except that the number of events observed in the SR is added as an input to the fit, and the BSM signal strength, constrained to be non-negative, is added as a free parameter. The observed and expected upper limits at 95% confidence level (CL) on the number of events from BSM phenomena for each signal region (S^{95}_{obs} and S^{95}_{exp}) are derived using the CL_{s} prescription [77], neglecting any possible signal contamination in the control regions. These limits, when normalized by the integrated luminosity of the data sample, may be interpreted as upper limits on the visible cross-section of BSM physics ($\langle \epsilon\sigma \rangle^{95}_{\mathrm{obs}}$), where the visible cross-section is

defined as the product of production cross-section, acceptance and efficiency. The model-independent fit is also used to compute the one-sided p-value (p_0) of the background-only hypothesis which quantifies the statistical significance of an excess.

Finally, model-dependent fits are used to set exclusion limits on the signal cross-sections for specific SUSY models. Such a fit proceeds in the same way as the model-independent fit, except that signal contamination in the CRs is taken into account as well as the yield in the signal region. Correlations between signal and background systematic uncertainties are taken into account where appropriate.

6 Event selection

This analysis searches for the production of heavy SUSY particles decaying into jets and stable lightest neutralinos, with the latter creating missing transverse momentum. Because of the high mass scale expected for the SUSY signal, the 'effective mass', m_{eff}, is a powerful discriminant between the signal and most SM backgrounds. When selecting events with at least N_{j} jets, $m_{\text{eff}}(N_{\text{j}})$ is defined to be the scalar sum of the transverse momenta of the leading N_{j} jets and $E_{\text{T}}^{\text{miss}}$. The final signal selection uses requirements on m_{eff}(incl.), which sums over all jets with $p_{\text{T}} > 50$ GeV and $E_{\text{T}}^{\text{miss}}$. Requirements placed on m_{eff} and $E_{\text{T}}^{\text{miss}}$ form the basis of this search by strongly suppressing the multi-jet background where the jet energy mismeasurement generates missing transverse momentum.

Following the object reconstruction described in Section 4, events are discarded if a baseline electron or muon with $p_{\text{T}} > 10$ GeV remains, or if they contain a jet failing quality selection criteria designed to suppress detector noise and non-collision backgrounds (described in Section 4). After these selections, only jets with $p_{\text{T}} > 50$ GeV are considered. Reconstructed photons and taus are not used in SR selections.

In order to achieve good reach over the $(m_{\tilde{g}}, m_{\tilde{q}})$-plane, a variety of signal regions are defined. Squarks typically generate at least one jet in their decays, for instance through $\tilde{q} \to q\tilde{\chi}_1^0$, while gluinos typically generate at least two jets, for instance through $\tilde{g} \to q\bar{q}\tilde{\chi}_1^0$. Processes contributing to $\tilde{q}\tilde{q}$ and $\tilde{g}\tilde{g}$ final states therefore lead to events containing at least two or four jets, respectively. Decays of heavy SUSY and SM particles produced in longer $\tilde{q}$ and $\tilde{g}$ cascade decays (e.g. $\tilde{\chi}_1^{\pm} \to qq'\tilde{\chi}_1^0$) tend to further increase the jet multiplicity in the final state.

Seven inclusive SRs characterised by increasing minimum jet-multiplicity from two to six, are defined in Table 2. Several SRs may be defined for the same jet-multiplicity requirement, distinguished by increasing background rejection, ranging from 'loose' (labelled 'l') to 'tight' (labelled 't').

Requirements are placed upon $\Delta\phi(\text{jet}, \boldsymbol{E}_{\text{T}}^{\text{miss}})_{\text{min}}$, which is defined to be the smallest azimuthal separation between $\boldsymbol{E}_{\text{T}}^{\text{miss}}$ and the reconstructed jets. For the SRs which are optimised for squark-pair (gluino-pair) production followed by the direct decay of squarks (gluinos), the selection requires $\Delta\phi(\text{jet}, \boldsymbol{E}_{\text{T}}^{\text{miss}})_{\text{min}} > 0.8$ ($\Delta\phi(\text{jet}, \boldsymbol{E}_{\text{T}}^{\text{miss}})_{\text{min}} > 0.4$) using up to three leading jets present in the event. For the SRs requiring at least four jets in the final state, an additional requirement $\Delta\phi(\text{jet}, \boldsymbol{E}_{\text{T}}^{\text{miss}})_{\text{min}} > 0.2$ is placed on all jets. Requirements on $\Delta\phi(\text{jet}, \boldsymbol{E}_{\text{T}}^{\text{miss}})_{\text{min}}$ and $E_{\text{T}}^{\text{miss}}/m_{\text{eff}}(N_{\text{j}})$ are designed to reduce the background from multi-jet processes. Signal region 2jm makes use of the presence of initial-state radiation jets by requiring a higher p_{T} threshold on the most energetic jet in the event, and is optimised to target models with small mass differences between the SUSY particles (compressed scenarios).

In the 2-jet SRs the requirement on $E_{\mathrm{T}}^{\mathrm{miss}}/m_{\mathrm{eff}}(N_{\mathrm{j}})$ is replaced by a requirement on $E_{\mathrm{T}}^{\mathrm{miss}}/\sqrt{H_{\mathrm{T}}}$ (where H_{T} is defined as the scalar sum of the transverse momenta of all jets), which was found to lead to enhanced sensitivity to models characterised by $\tilde{q}\tilde{q}$ production. In the other regions additional suppression of background processes is based on the aplanarity variable which is defined as $A = 3/2\lambda_3$, where λ_3 is the smallest eigenvalue of the normalised momentum tensor of the jets [78].

Table 2: Selection criteria used to define each of the signal regions in the analysis. Each SR is labelled with the inclusive jet multiplicity considered ('2j', '4j' etc.) together with the degree of background rejection. The latter is denoted by labels 'l' ('loose'), 'm' ('medium') and 't' ('tight'). The $E_{\mathrm{T}}^{\mathrm{miss}}/m_{\mathrm{eff}}(N_{\mathrm{j}})$ cut in any N_{j}-jet channel uses a value of m_{eff} constructed from only the leading N_{j} jets ($m_{\mathrm{eff}}(N_{\mathrm{j}})$). However, the final m_{eff}(incl.) selection, which is used to define the signal regions, includes all jets with $p_{\mathrm{T}} > 50$ GeV.

Requirement	Signal Region						
	2jl	**2jm**	**2jt**	**4jt**	**5j**	**6jm**	**6jt**
$E_{\mathrm{T}}^{\mathrm{miss}}$ [GeV] >	200						
$p_{\mathrm{T}}(j_1)$ [GeV] >	200	300	200				
$p_{\mathrm{T}}(j_2)$ [GeV] >	200	50	200	100			
$p_{\mathrm{T}}(j_3)$ [GeV] >	–			100			
$p_{\mathrm{T}}(j_4)$ [GeV] >	–			100			
$p_{\mathrm{T}}(j_5)$ [GeV] >	–				100		
$p_{\mathrm{T}}(j_6)$ [GeV] >	–					100	
$\Delta\phi(\mathrm{jet}_{1,2,(3)}, \boldsymbol{E}_{\mathrm{T}}^{\mathrm{miss}})_{\mathrm{min}}$ >	0.8	0.4	0.8	0.4			
$\Delta\phi(\mathrm{jet}_{i>3}, \boldsymbol{E}_{\mathrm{T}}^{\mathrm{miss}})_{\mathrm{min}}$ >	–			0.2			
$E_{\mathrm{T}}^{\mathrm{miss}}/\sqrt{H_{\mathrm{T}}}$ [GeV$^{1/2}$] >	15		20	–			
Aplanarity >	–			0.04			
$E_{\mathrm{T}}^{\mathrm{miss}}/m_{\mathrm{eff}}(N_{\mathrm{j}})$ >	–			0.2	0.25		0.2
m_{eff}(incl.) [GeV] >	1200	1600	2000	2200	1600	1600	2000

7 Background estimation

Standard Model background processes contribute to the event counts in the signal regions. The dominant sources are: Z+jets, W+jets, top quark pairs, single top quarks, and the multi-jet production. The diboson production is estimated with MC simulated data normalised to NLO cross-section predictions, as described in Section 3. The majority of the W+jets background is composed of $W \to \tau\nu$ events in which the τ-lepton decays to hadrons, with additional contributions from $W \to e\nu, \mu\nu$ events in which no baseline electron or muon is reconstructed. The largest part of the Z+jets background comes from the irreducible component in which $Z \to \nu\bar{\nu}$ decays generate large $E_{\mathrm{T}}^{\mathrm{miss}}$. Top quark pair production followed by semileptonic decays, in particular $t\bar{t} \to b\bar{b}\tau\nu qq'$ (with the τ-lepton decaying to hadrons), as well as single top quark events, can also generate large $E_{\mathrm{T}}^{\mathrm{miss}}$ and satisfy the jet and lepton-veto requirements at a non-negligible rate. The multi-jet background in the signal regions is caused by mis-reconstruction of jet energies in the calorimeters generating missing transverse momentum, as well as by neutrino production

in semileptonic decays of heavy-flavour quarks. After applying requirements based on $\Delta\phi(\text{jet}, \boldsymbol{E}_{\text{T}}^{\text{miss}})_{\text{min}}$ and $E_{\text{T}}^{\text{miss}}/m_{\text{eff}}(N_{\text{j}})$ listed in Table 2 the remaining multi-jet background is negligible.

Table 3: Control regions used in the analysis. Also listed are the main targeted background in the SR in each case, the process used to model the background, and the main CR requirement(s) used to select this process. The transverse momenta of high-purity leptons (photons) used to select CR events must exceed 25 (130) GeV.

CR	SR background	CR process	CR selection
CRγ	$Z(\rightarrow \nu\bar{\nu})$+jets	γ+jets	Isolated photon
CRQ	Multi-jet	Multi-jet	SR with reversed requirements on (i) $\Delta\phi(\text{jet}, \boldsymbol{E}_{\text{T}}^{\text{miss}})_{\text{min}}$ and (ii) $E_{\text{T}}^{\text{miss}}/m_{\text{eff}}(N_{\text{j}})$ or $E_{\text{T}}^{\text{miss}}/\sqrt{H_{\text{T}}}$
CRW	$W(\rightarrow \ell\nu)$+jets	$W(\rightarrow \ell\nu)$+jets	30 GeV $< m_{\text{T}}(\ell, E_{\text{T}}^{\text{miss}}) <$ 100 GeV, b-veto
CRT	$t\bar{t}$(+EW) and single top	$t\bar{t} \rightarrow b\bar{b}qq'\ell\nu$	30 GeV $< m_{\text{T}}(\ell, E_{\text{T}}^{\text{miss}}) <$ 100 GeV, b-tag

In order to estimate the backgrounds in a consistent and robust fashion, four control regions are defined for each of the seven signal regions, giving 28 CRs in total. The CR selections are optimised to maintain adequate statistical precision while minimising as much as possible the systematic uncertainties arising from the extrapolation of the CR event yield to the expectation in the SR. This latter requirement is addressed through the use of CR jet p_{T} thresholds and m_{eff}(incl.) selections which match those used in the SR. The CR definitions are listed in Table 3. The CRγ region is used to estimate the contribution of $Z(\rightarrow \nu\bar{\nu})$+jets background events to each SR by selecting a sample of γ+jets events with $p_{\text{T}}(\gamma) > 130$ GeV and then treating the reconstructed photon as contributing to $E_{\text{T}}^{\text{miss}}$. For $p_{\text{T}}(\gamma)$ significantly larger than m_Z the kinematics of such events strongly resemble those of Z+jets events [13]. A correction factor is applied to the CRγ events to reduce the theoretical uncertainties associated with the SR Z/γ^*+jets background expectations arising from the use of LO γ+jets cross-sections. This correction factor, $\kappa = 1.6 \pm 0.1$, is determined by comparing CRγ observations with those in a highly populated auxiliary control region defined by selecting events with a low-p_{T} Z boson decaying to electrons or muons (200 GeV $< |\boldsymbol{E}_{\text{T}}^{\text{miss}} + \boldsymbol{p}_{\text{T}}(\ell\bar{\ell})| <$ 300 GeV), together with at least two jets. The CRQ region uses reversed selection requirements on $\Delta\phi(\text{jet}, \boldsymbol{E}_{\text{T}}^{\text{miss}})_{\text{min}}$ and on $E_{\text{T}}^{\text{miss}}/m_{\text{eff}}(N_{\text{j}})$ ($E_{\text{T}}^{\text{miss}}/\sqrt{H_{\text{T}}}$ where appropriate) to produce data samples enriched in multi-jet background events. The CRW and CRT regions use respectively a b-jet veto or require the presence of at least one b-jet together with a requirement on the transverse mass m_{T} of a high-purity lepton with $p_{\text{T}} > 25$ GeV and $\boldsymbol{E}_{\text{T}}^{\text{miss}}$ to select samples rich in $W(\rightarrow \ell\nu)$+jets and semileptonic $t\bar{t}$ background events. These samples are used to estimate respectively the W+jets and combined $t\bar{t}$ and single top background populations, treating the lepton as a jet with the same momentum to model background events in which a hadronically decaying τ-lepton is produced. The CRW and CRT selections do not use the SR selection requirements on $\Delta\phi(\text{jet}, \boldsymbol{E}_{\text{T}}^{\text{miss}})_{\text{min}}$ or $E_{\text{T}}^{\text{miss}}/m_{\text{eff}}(N_{\text{j}})$ ($E_{\text{T}}^{\text{miss}}/\sqrt{H_{\text{T}}}$ where appropriate) in order to increase CR data event statistics without significantly increasing the theoretical uncertainties associated with the background estimation procedure.

As an example, the m_{eff}(incl.) distributions in control regions associated with SR4jt are shown in Figure 2. In all CRs, the data is consistent with the pre-fit MC within uncertainties, although the overall normalization tends to be lower by approximately one standard deviation.

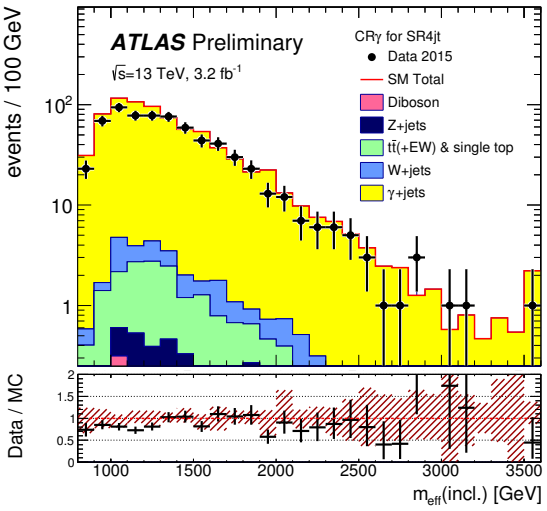

(a)

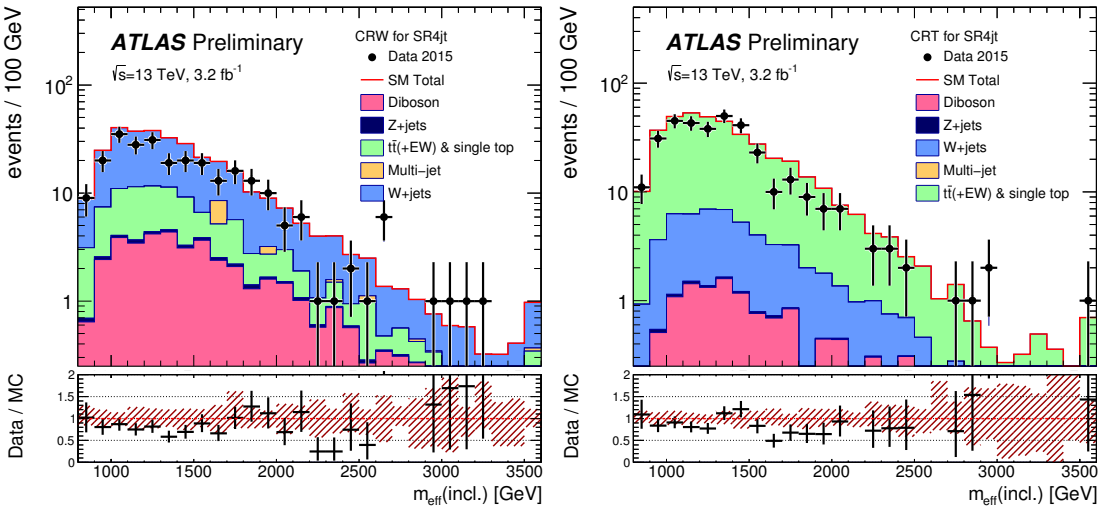

(b) (c)

Figure 2: Observed m_{eff}(incl.) distributions in control regions (a) CRγ, (b) CRW and (c) CRT after selecting events with $E_{\text{T}}^{\text{miss}} > 200$ GeV and at least four energetic jets with the corresponding transverse momenta as indicated in Table 2 for SR4jt. The histograms denote the pre-fit MC background expectations, normalised to cross-section times integrated luminosity. The last bin includes the overflow. In the lower panels the hatched (red) error bands denote the combined experimental, MC statistical and theoretical modelling uncertainties.

8 Systematic uncertainties

Systematic uncertainties on background estimates arise from the use of extrapolation factors which relate observations in the control regions to background expectations in the signal regions, and from the MC modelling of minor backgrounds.

The overall background uncertainties, detailed in Table 4, range from 9% in SR 2jl, where the loose selection minimises theoretical uncertainties and the impact of statistical fluctuations in the CRs, to 29% in SR 6jt.

For the backgrounds estimated with MC simulation-derived extrapolation factors the primary common sources of systematic uncertainty are the JES calibration, jet energy resolution (JER), theoretical uncertainties, and limited event yields in the MC samples and data CRs. Correlations between uncertainties (for instance between JES uncertainties in CRs and SRs) are taken into account where appropriate.

The JES uncertainty was measured using the techniques described in Refs. [65, 68, 79], leading to a slight dependence upon p_{T} and η. The JER uncertainty is estimated using the methods discussed in Ref. [80]. Contributions are added to both the JES and the JER uncertainties to account for the effect of pile-up at the relatively high luminosity delivered by the LHC in the 2015 run. A further uncertainty originating from the tracks not associated to the reconstructed objects but included in the $E_{\mathrm{T}}^{\mathrm{miss}}$ calculation is taken into account. The combined JES, JER and $E_{\mathrm{T}}^{\mathrm{miss}}$ uncertainty ranges from 1% of the expected background in 2-jet SRs to 9% in SR 6jt.

Uncertainties arising from theoretical modelling of background processes are evaluated by comparing samples produced with different MC generators. The W/Z+jets events generated with Sherpa are compared to events generated with Madgraph 5.2.2.2 at leading order interfaced to the Pythia 8.186 parton shower model. The uncertainty of the modelling of top quark pair production are estimated by comparing Powheg-Box to aMc@Nlo [81], and by accounting for different generator and radiation tunes. Uncertainties on diboson production due to scale and PDF uncertainties are accounted for by applying a uniform 50% uncertainty in all SRs, and are the dominant source of uncertainty in SRs 2jl and 2jm. The largest uncertainties are associated with the modelling of the Z+jets production in the SRs with tight selections cuts (up to 20%). The statistical uncertainty arising from the use of finite-size MC samples is largest (9%) in SR 6jt. The uncertainties arising from the data-driven correction procedure applied to events selected in the CRγ region, described in Section 7, are included in Table 4 under 'CRγ corr. factor' and reach a maximal value of 4% in signal regions 2jm and 2jt. The impact of lepton reconstruction uncertainties, and of the uncertainties related to the b-tag/b-veto efficiency on the overall background uncertainty are expected to be negligible for all SRs, and are presently not considered. The total background uncertainties for all SRs, broken down into the main contributing sources, are summarised in Table 4.

9 Results, interpretation and limits

The background estimation procedure is validated by comparing the numbers of events observed in the VRs to the corresponding SM background expectations obtained from the background-only fits. Several VR samples are selected with requirements distinct from those used in the CRs, which maintain a low probability of signal contamination. The CRγ estimates of the $Z(\rightarrow \nu\bar{\nu})$+jets background are validated using the samples of $Z(\rightarrow \ell\bar{\ell})$+jets events selected by requiring high-purity lepton pairs of opposite sign and identical flavour for which the dilepton invariant mass lies within 25 GeV of the mass of the Z

Table 4: Breakdown of the dominant systematic uncertainties on the background estimates. The individual uncertainties can be correlated, and do not necessarily add up quadratically to the total background uncertainty. $\Delta\mu$ uncertainties are the result of the control region statistical uncertainties and the systematic uncertainties entering a specific control region. In brackets, uncertainties are given relative to the expected total background yield. Empty cells (indicated by a '-') correspond to uncertainties lower than 1 per mil.

Channel	**2jl**	**2jm**	**2jt**	**4jt**	**5j**	**6jm**	**6jt**
Total bkg	237	163	20	3.5	11.7	5.5	3.1
Total bkg unc.	±22 [9%]	±20 [12%]	±5 [25%]	±0.8 [23%]	±2.2 [19%]	±1.2 [22%]	±0.9 [29%]
MC statistics	–	±1.8 [1%]	±0.5 [3%]	±0.26 [7%]	±0.5 [4%]	±0.35 [6%]	±0.27 [9%]
$\Delta\mu_{Z+\text{jets}}$	±6 [3%]	±5 [3%]	±2.0 [10%]	±0.5 [14%]	±0.8 [7%]	±0.6 [11%]	±0.4 [13%]
$\Delta\mu_{W+\text{jets}}$	±4 [2%]	±4 [2%]	±0.7 [3%]	±0.32 [9%]	±0.7 [6%]	±0.5 [9%]	±0.4 [13%]
$\Delta\mu_{\text{Top}}$	±1.2 [1%]	±1.6 [1%]	±0.21 [1%]	±0.26 [7%]	±0.32 [3%]	±0.21 [4%]	±0.24 [8%]
$\Delta\mu_{\text{Multi-jet}}$	±0.05 [0%]	±0.09 [0%]	–	–	–	–	–
CRγ corr. factor	±8 [3%]	±6 [4%]	±0.8 [4%]	±0.1 [3%]	±0.29 [2%]	±0.13 [2%]	±0.07 [2%]
Theory W	±1.4 [1%]	±2.3 [1%]	±0.4 [2%]	±0.22 [6%]	±0.7 [6%]	±0.4 [7%]	±0.34 [11%]
Theory Z	±6 [3%]	±3.2 [2%]	±4 [20%]	±0.32 [9%]	±0.9 [8%]	±0.32 [6%]	±0.3 [10%]
Theory Top	±2.7 [1%]	±2.1 [1%]	±0.5 [3%]	±0.24 [7%]	±0.2 [2%]	±0.27 [5%]	±0.2 [6%]
Theory Diboson	±16 [7%]	±16 [10%]	±2.0 [10%]	–	±1.0 [9%]	–	–
Jet/$E_{\text{T}}^{\text{miss}}$	±1.5 [1%]	±2.1 [1%]	±0.29 [1%]	±0.14 [4%]	±0.8 [7%]	±0.4 [7%]	±0.27 [9%]

boson. In this VR the leptons are treated as contributing to $E_{\text{T}}^{\text{miss}}$. The CRW and CRT estimates of the W+jets and top quark background are validated with the same CRW and CRT selections, but reinstating the requirement on $\Delta\phi(\text{jet}, \boldsymbol{E}_{\text{T}}^{\text{miss}})_{\text{min}}$ and $E_{\text{T}}^{\text{miss}}/m_{\text{eff}}(N_{\text{j}})$ (or $E_{\text{T}}^{\text{miss}}/\sqrt{H_{\text{T}}}$ as appropriate), and treating the lepton either as a jet or as contributing to $E_{\text{T}}^{\text{miss}}$. The CRQ estimates of the multi-jet background are validated with VRs for which the CRQ selection is applied, but with the SR $E_{\text{T}}^{\text{miss}}/m_{\text{eff}}(N_{\text{j}})$ ($E_{\text{T}}^{\text{miss}}/\sqrt{H_{\text{T}}}$) requirement reinstated, or with a requirement of an intermediate value of $\Delta\phi(\text{jet}, \boldsymbol{E}_{\text{T}}^{\text{miss}})_{\text{min}}$ applied. Most VR observations lie within 1 standard deviation (σ) of the background expectations, with the largest discrepancy of 1.9 σ in the VR used to validate the W+jets estimate in the 6jm region; this particular VR requires the same selections as the corresponding SR, except that a lepton is required and is treated as contributing to $E_{\text{T}}^{\text{miss}}$.

Distributions of m_{eff}(incl.) obtained before the final selections on this quantity (but after applying all other selections), for data and the different MC samples normalised with the theoretical cross-sections, i.e. before applying the normalisation from the CR fit, are shown in Figures 3–4. Examples of typical expected SUSY signals are shown for illustration. These signals correspond to the processes to which each SR is primarily sensitive – $\tilde{q}\tilde{q}$ production for the lower jet-multiplicity SRs and $\tilde{g}\tilde{g}$ production for the higher jet-multiplicity SRs. In these figures data and background distributions largely agree within uncertainties.

The number of events observed in the data and the number of SM events expected to enter each of the signal regions, determined using the background-only fit, are shown in Table 5 and Figure 5. The pre-fit background expectations are also shown in Table 5 for comparison. The fit to the CRs for each SR compensates for the differences related to the overall normalization of the background seen in Figures 3–4, leading to good agreement between data and post-fit expectations.

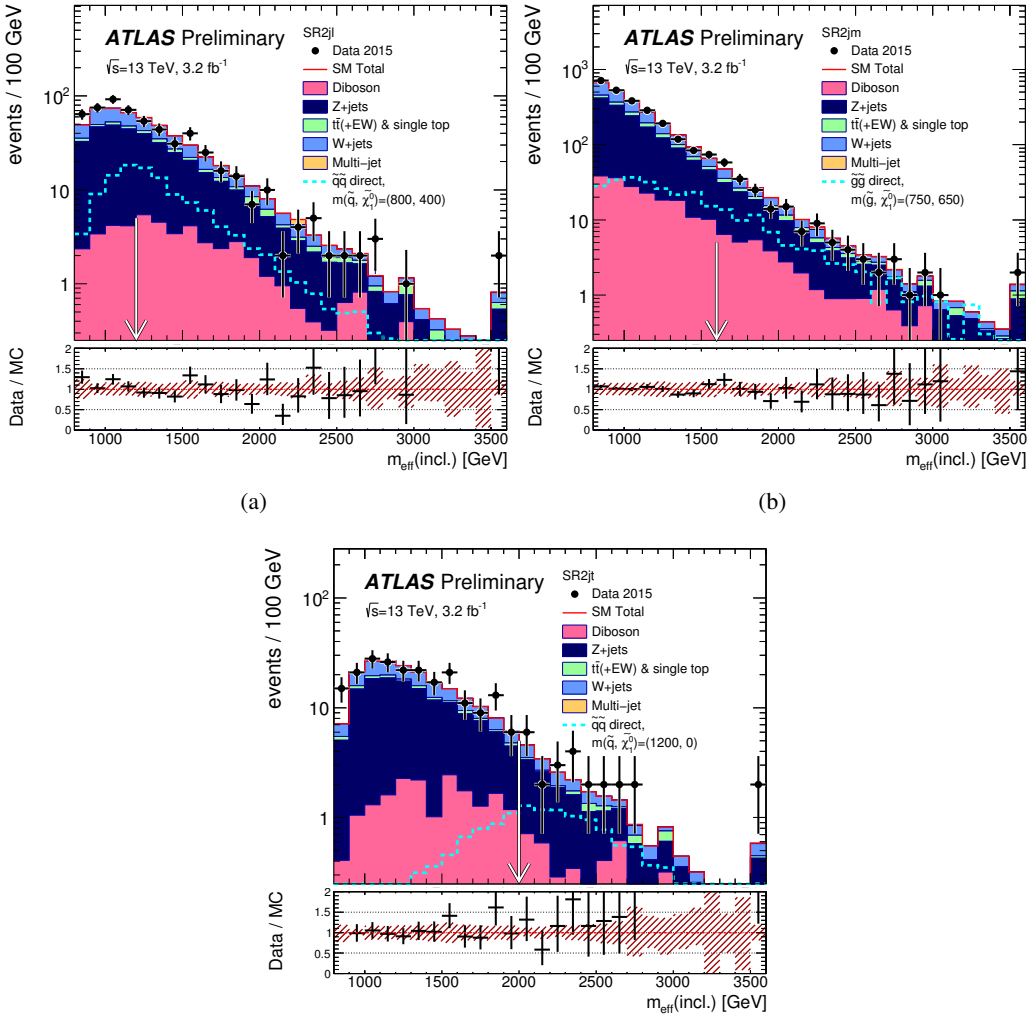

Figure 3: Observed m_{eff}(incl.) distributions for the 2-jet signal regions. The histograms denote the MC background expectations prior to the fits described in the text, normalised to cross-section times integrated luminosity. The last bin includes the overflow. In the lower panels the hatched (red) error bands denote the combined experimental, MC statistical and theoretical modelling uncertainties. The arrows indicate the values at which the requirements on m_{eff}(incl.) are applied. Expected distributions for benchmark model points are also shown for comparison (masses in GeV).

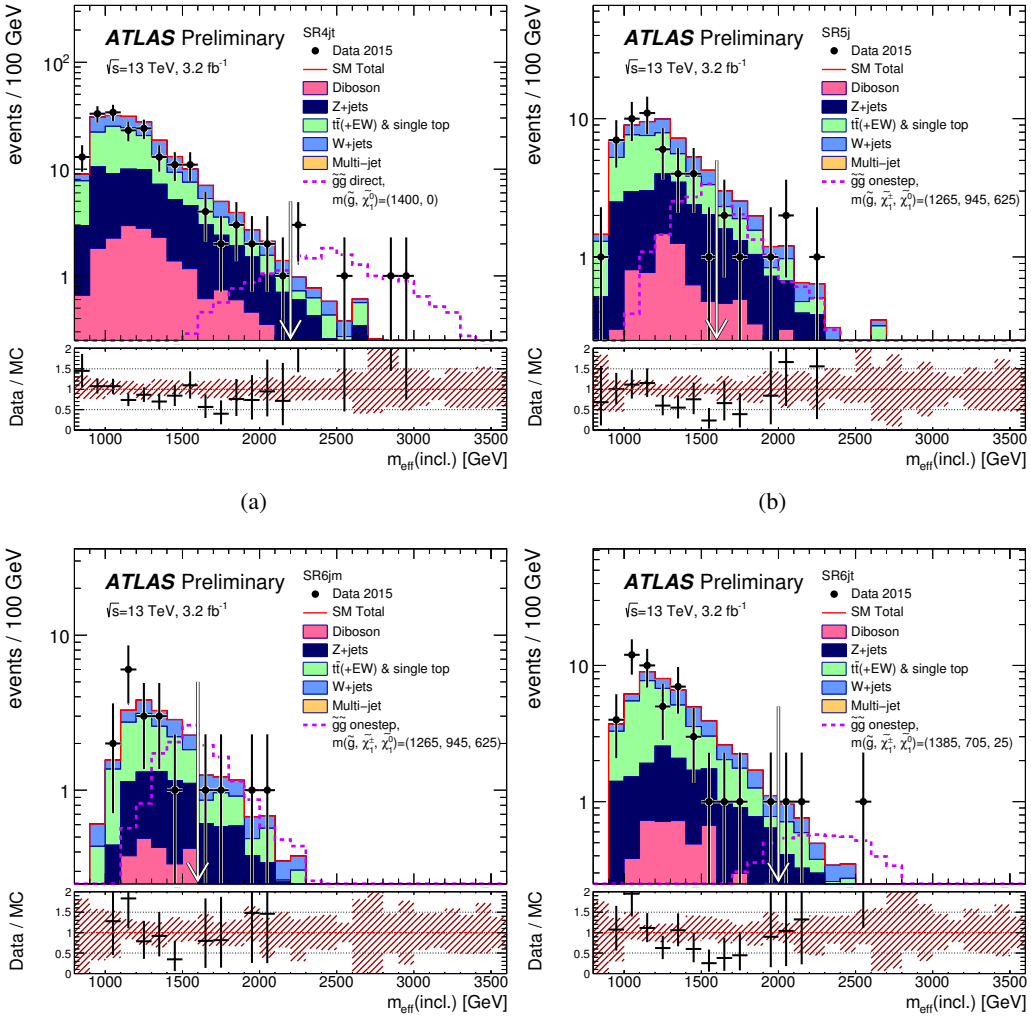

Figure 4: Observed m_{eff}(incl.) distributions for the (a) 4jt, (b) 5j, (c) 6jm and (d) 6jt signal regions. The histograms denote the MC background expectations prior to the fits described in the text, normalised to cross-section times integrated luminosity. The last bin includes the overflow. In the lower panels the hatched (red) error bands denote the combined experimental, MC statistical and theoretical modelling uncertainties. The arrows indicate the values at which the requirements on m_{eff}(incl.) are applied. Expected distributions for benchmark model points are also shown for comparison (masses in GeV).

Table 5: Numbers of events observed in the signal regions used in the analysis compared with background expectations obtained from the fits described in the text. No signal contribution is considered in the CRs for the fit. Empty cells (indicated by a '-') correspond to estimates lower than 0.01. The p-values (p_0) give the probabilities of the observations being consistent with the estimated backgrounds and are bounded above by 0.5. Between parenthesis, p-values are also given in number of equivalent Gaussian sigma (Z). Also shown are 95% CL upper limits on the visible cross-section ($\langle\epsilon\sigma\rangle^{95}_{\rm obs}$), the visible number of signal events ($S^{95}_{\rm obs}$) and the number of signal events ($S^{95}_{\rm exp}$) given the expected number of background events (and $\pm1\sigma$ excursions on the expectation).

Signal Region	**2jl**	**2jm**	**2jt**	**4jt**	**5j**	**6jm**	**6jt**
MC expected events							
Diboson	33	33	4.0	0.7	2.4	1.1	0.5
Z/γ^*+jets	151	94	12	1.8	4.9	2.5	1.3
W+jets	72	42	4.5	0.9	3.0	1.6	0.9
$t\bar{t}$(+EW) + single top	18	17	1.2	0.9	2.7	1.6	1.1
Multi-jet	0.6	0.8	0.03	–	–	–	–
Total MC	275	188	22	4.3	13	6.7	3.8
Fitted background events							
Diboson	33 ± 17	33 ± 17	4.0 ± 2.0	0.67 ± 0.35	2.4 ± 1.3	1.1 ± 0.6	0.5 ± 0.4
Z/γ^*+jets	127 ± 12	85 ± 8	12 ± 4	1.5 ± 0.6	4.5 ± 1.3	2.0 ± 0.7	1.1 ± 0.6
W+jets	61 ± 4	32 ± 5	2.9 ± 0.8	0.7 ± 0.4	3.3 ± 1.0	1.7 ± 0.7	1.0 ± 0.6
$t\bar{t}$(+EW) + single top	14.6 ± 2.9	10.5 ± 2.6	0.7 ± 0.5	0.6 ± 0.4	1.4 ± 0.5	0.8 ± 0.4	0.46 ± 0.33
Multi-jet	0.51 ± 0.06	0.6 ± 0.5	–	–	–	–	–
Total bkg	237 ± 22	163 ± 20	20 ± 5	3.5 ± 0.8	11.7 ± 2.2	5.5 ± 1.2	3.1 ± 0.9
Observed	264	186	25	6	7	4	3
$\langle\epsilon\sigma\rangle^{95}_{\rm obs}$ [fb]	24	21	5.9	2.5	2.0	1.6	1.6
$S^{95}_{\rm obs}$	76	67	19	8.2	6.3	5.3	5.0
$S^{95}_{\rm exp}$	52^{+22}_{-15}	46^{+19}_{-12}	$14.1^{+5.1}_{-3.1}$	$5.7^{+2.2}_{-1.6}$	$8.5^{+3.3}_{-2.1}$	$6.5^{+2.5}_{-1.6}$	$5.0^{+2.3}_{-1.4}$
p_0 (Z)	0.11 (1.20)	0.12 (1.15)	0.18 (0.93)	0.14 (1.08)	0.5 (0.0)	0.5 (0.0)	0.5 (0.0)

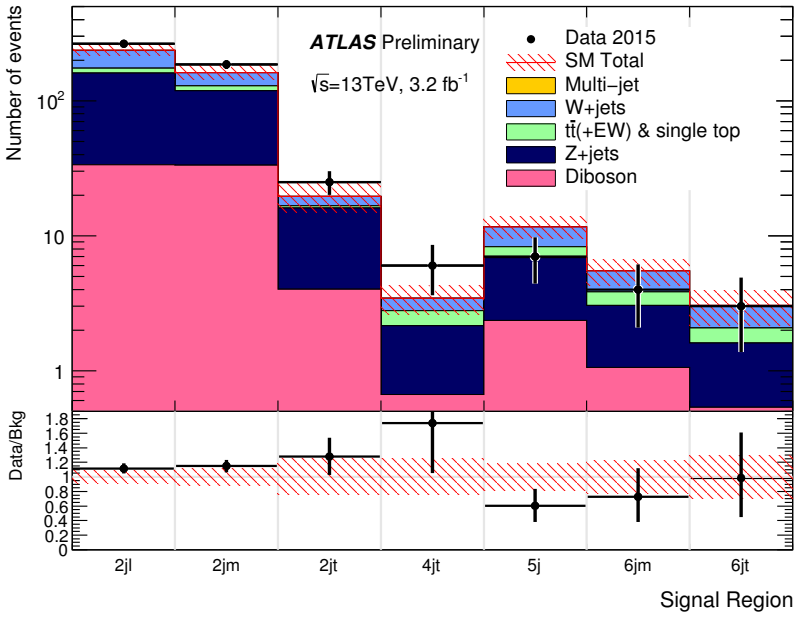

Figure 5: Comparison of the observed and expected event yields as a function of signal region. The background expectations are those obtained from the background-only fits, presented in Table 5.

In the absence of a statistically significant excess, limits are set on contributions to the SRs from BSM physics. Upper limits at 95% CL on the number of BSM signal events in each SR and the corresponding visible BSM cross-section are derived from the model-independent fits described in Section 5 using the CL_s prescription. The results are presented in Table 5.

The model-dependent fits in all the SRs are then used to set limits on specific classes of SUSY models, using the result from the SR with the best expected sensitivity at each point in each model parameter space. 'Observed limits' are calculated from the observed SR event yields for the nominal signal cross-section. 'Expected limits' are calculated by setting the nominal event yield in each SR to the corresponding mean expected background.

In Figure 6 limits are shown for two classes of simplified model in which only direct production of light-flavour squark or gluino pairs are considered. In these simplified model scenarios, the lower limit on the light-flavour squark mass is 980 GeV assuming massless $\tilde{\chi}_1^0$, as obtained from the signal region 2jt. The corresponding limit on the gluino mass is 1520 GeV, when the $\tilde{\chi}_1^0$ is massless, as obtained from the signal region 4jt.

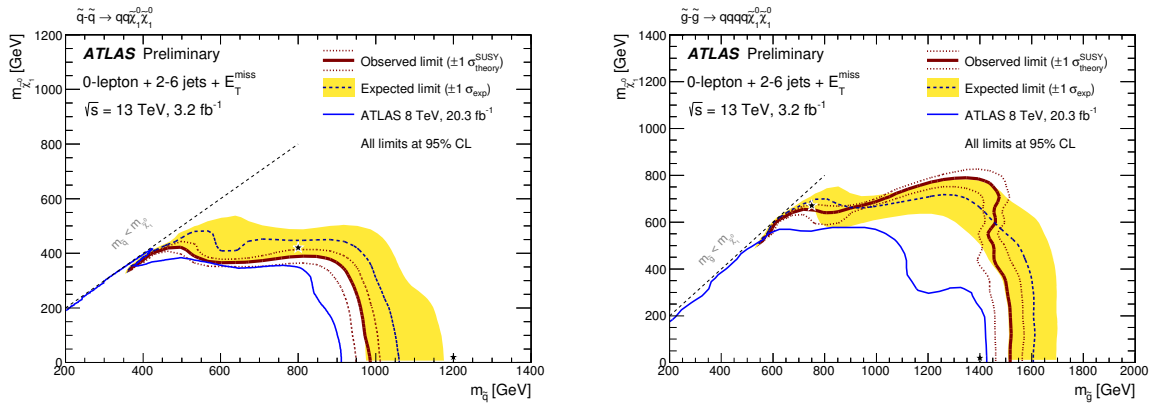

(a) (b)

Figure 6: Exclusion limits for direct production of (a) light-flavour squark pairs with decoupled gluinos and (b) gluino pairs with decoupled squarks. Gluinos (light-flavour squarks) are required to decay to two quarks (one quark) and a neutralino LSP. Exclusion limits are obtained by using the signal region with the best expected sensitivity at each point. The blue dashed lines show the expected limits at 95% CL, with the light (yellow) bands indicating the 1σ excursions due to experimental and background-only theoretical uncertainties. Observed limits are indicated by medium dark (maroon) curves where the solid contour represents the nominal limit, and the dotted lines are obtained by varying the signal cross-section by the renormalisation and factorisation scale and PDF uncertainties. Results are compared with the observed limits obtained by previous ATLAS search [15]. The black stars indicate the benchmark models used in Figures 3–4.

In Figure 7 limits are shown for pair-produced gluinos each decaying via an intermediate $\tilde{\chi}_1^\pm$ to two quarks, a W boson and a $\tilde{\chi}_1^0$. Results are presented for simplified models in which the mass splitting between the $\tilde{\chi}_1^\pm$ and the $\tilde{\chi}_1^0$ is related to that between the gluino and the $\tilde{\chi}_1^0$, and is fixed to $m(\tilde{\chi}_1^\pm) = (m(\tilde{g}) + m(\tilde{\chi}_1^0))/2$. For a $\tilde{\chi}_1^0$ mass of $\sim$ 200 GeV, the lower limit on the gluino mass, obtained from the signal region 6jt, extends up to 1510 GeV in this model.

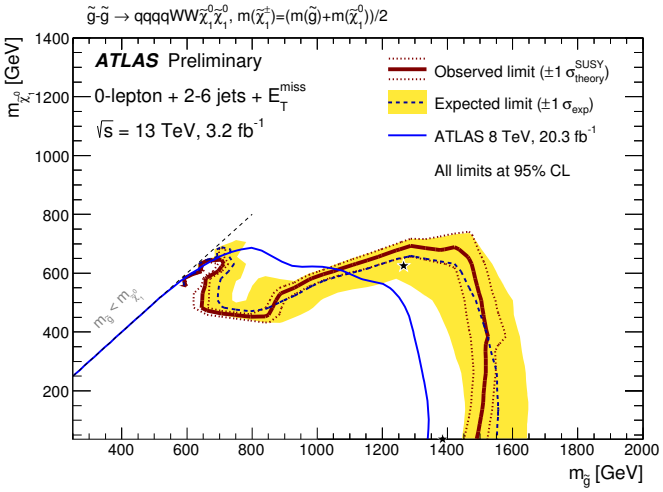

Figure 7: Exclusion limits for pair-produced gluinos each decaying via an intermediate $\tilde{\chi}_1^\pm$ to two quarks, a W boson and a $\tilde{\chi}_1^0$ for models with a fixed $m(\tilde{\chi}_1^\pm) = (m(\tilde{g}) + m(\tilde{\chi}_1^0))/2$ and varying values of $m(\tilde{g})$ and $m(\tilde{\chi}_1^0)$. Exclusion limits are obtained by using the signal region with the best expected sensitivity at each point. The blue dashed lines show the expected limits at 95% CL, with the light (yellow) bands indicating the 1σ excursions due to experimental and background-only theoretical uncertainties. Observed limits are indicated by medium dark (maroon) curves where the solid contour represents the nominal limit, and the dotted lines are obtained by varying the signal cross-section by the renormalisation and factorisation scale and PDF uncertainties. Results are compared with the observed limits obtained by previous ATLAS search [15]. The black stars indicate the benchmark models used in Figure 4.

10 Conclusion

This document reports a search for squarks and gluinos in final states containing high-p_{T} jets, large missing transverse momentum and no electrons or muons, based on a 3.2 fb^{-1} dataset of $\sqrt{s} = 13$ TeV proton–proton collisions recorded by the ATLAS experiment at the LHC in 2015. Good agreement is seen between the numbers of events observed in the data and the numbers of events expected from SM processes.

Results are interpreted in terms of simplified models with only light-flavour squarks, or gluinos, together with a neutralino LSP, with the masses of all the other SUSY particles set beyond the reach of the LHC. For a massless lightest neutralino, gluino masses below 1520 GeV are excluded at the 95% confidence level in a simplified model with only gluinos and the lightest neutralino. For a simplified model involving the strong production of squarks of the first and second generations, with decays to a massless lightest neutralino, squark masses below 980 GeV are excluded, assuming mass degenerate squarks. In simplified models with pair-produced gluinos, each decaying via an intermediate $\tilde{\chi}_1^\pm$ to two quarks, a W boson and a $\tilde{\chi}_1^0$, gluino masses below 1510 GeV are excluded for $\tilde{\chi}_1^0$ masses of $\sim$ 200 GeV. These results extend the region of supersymmetric parameter space excluded by previous LHC searches.

References

[1] Y. A. Golfand and E. P. Likhtman,
Extension of the Algebra of Poincare Group Generators and Violation of p Invariance,
JETP Lett. **13** (1971) 323, [Pisma Zh.Eksp.Teor.Fiz.13:452-455,1971].

[2] D. V. Volkov and V. P. Akulov, *Is the Neutrino a Goldstone Particle?*,
Phys. Lett. **B 46** (1973) 109.

[3] J. Wess and B. Zumino, *Supergauge Transformations in Four-Dimensions*,
Nucl. Phys. **B 70** (1974) 39.

[4] J. Wess and B. Zumino, *Supergauge Invariant Extension of Quantum Electrodynamics*,
Nucl. Phys. **B78** (1974) 1.

[5] S. Ferrara and B. Zumino, *Supergauge Invariant Yang-Mills Theories*,
Nucl. Phys. **B79** (1974) 413.

[6] A. Salam and J. A. Strathdee, *Supersymmetry and Nonabelian Gauges*,
Phys. Lett. **B51** (1974) 353.

[7] G. R. Farrar and P. Fayet, *Phenomenology of the Production, Decay, and Detection of New Hadronic States Associated with Supersymmetry*, Phys. Lett. **B 76** (1978) 575.

[8] L. Evans and P. Bryant, *LHC Machine*, *JINST* **3** (2008) S08001.

[9] P. Fayet, *Supersymmetry and Weak, Electromagnetic and Strong Interactions*,
Phys. Lett. **B 64** (1976) 159.

[10] P. Fayet, *Spontaneously Broken Supersymmetric Theories of Weak, Electromagnetic and Strong Interactions*, Phys. Lett. **B 69** (1977) 489.

[11] ATLAS Collaboration, *Search for squarks and gluinos using final states with jets and missing transverse momentum with the ATLAS detector in* $\sqrt{s} = 7$ *TeV proton-proton collisions*,
Phys. Lett. **B 701** (2011) 186, arXiv: 1102.5290 [hep-ex].

[12] ATLAS Collaboration, *Search for squarks and gluinos using final states with jets and missing transverse momentum with the ATLAS detector in* $\sqrt{s} = 7$ *TeV proton-proton collisions*,
Phys. Lett. **B 710** (2012) 67, arXiv: 1109.6572 [hep-ex].

[13] ATLAS Collaboration,
Search for squarks and gluinos with the ATLAS detector in final states with jets and missing transverse momentum using 4.7 fb^{-1} *of* $\sqrt{s} = 7$ *TeV proton-proton collision data*,
Phys. Rev. **D 87** (2013) 012008, arXiv: 1208.0949 [hep-ex].

[14] ATLAS Collaboration, *Search for squarks and gluinos with the ATLAS detector in final states with jets and missing transverse momentum using* $\sqrt{s} = 8$ *TeV proton–proton collision data*,
JHEP **1409** (2014) 176, arXiv: 1405.7875 [hep-ex].

[15] ATLAS Collaboration, *Summary of the searches for squarks and gluinos using* $\sqrt{s} = 8$ *TeV pp collisions with the ATLAS experiment at the LHC*, JHEP **10** (2015) 054,
arXiv: 1507.05525 [hep-ex].

[16] CMS Collaboration,
Search for supersymmetry in hadronic final states using MT2 in pp collisions at $\sqrt{s} = 7$ *TeV*,
JHEP **10** (2012) 018, arXiv: 1207.1798 [hep-ex].

[17] CMS Collaboration, *Search for new physics in the multijet and missing transverse momentum final state in proton-proton collisions at* $\sqrt{s}$ = 7 *TeV*, *Phys. Rev. Lett.* **109** (2012) 171803, arXiv: 1207.1898 [hep-ex].

[18] CMS Collaboration, *Search for supersymmetry in hadronic final states with missing transverse energy using the variables* α_T *and b-quark multiplicity in pp collisions at 8 TeV*, *Eur. Phys. J.* **C 73** (2013) 2568, arXiv: 1303.2985 [hep-ex].

[19] CMS Collaboration, *Inclusive search for supersymmetry using the razor variables in pp collisions at* $\sqrt{s}$ = 7 *TeV*, *Phys. Rev. Lett.* **111** (2013) 081802, arXiv: 1212.6961 [hep-ex].

[20] CMS Collaboration, *Search for new physics in the multijet and missing transverse momentum final state in proton-proton collisions at* $\sqrt{s}$= *8 TeV*, JHEP **06** (2014) 055, arXiv: 1402.4770 [hep-ex].

[21] CMS Collaboration, *Searches for Supersymmetry using the* M_{T2} *Variable in Hadronic Events Produced in pp Collisions at 8 TeV*, JHEP **05** (2015) 078, arXiv: 1502.04358 [hep-ex].

[22] ATLAS Collaboration, *Search for gluinos in events with an isolated lepton, jets and missing transverse momentum at* $\sqrt{s}$ *=13 TeV with the ATLAS detector*, ATLAS-CONF-2015-076 (2015), URL: http://atlas.web.cern.ch/Atlas/GROUPS/PHYSICS/CONFNOTES/ATLAS-CONF-2015-076.

[23] J. Alwall et al., *Searching for Directly Decaying Gluinos at the Tevatron*, Phys. Lett. **B666** (2008) 34, arXiv: 0803.0019 [hep-ph].

[24] J. Alwall, P. Schuster and N. Toro, *Simplified Models for a First Characterization of New Physics at the LHC*, Phys. Rev. **D79** (2009) 075020, arXiv: 0810.3921 [hep-ph].

[25] D. Alves et al., *Simplified Models for LHC New Physics Searches*, J. Phys. G: Nucl. Part. Phys. **39** (2012) 105005, arXiv: 1105.2838 [hep-ph].

[26] ATLAS Collaboration, *The ATLAS Experiment at the CERN Large Hadron Collider*, JINST **3** (2008) S08003.

[27] ATLAS Collaboration, *ATLAS Insertable B-Layer Technical Design Report*, ATLAS-TDR-19 (2010), URL: http://cdsweb.cern.ch/record/1291633.

[28] ATLAS Collaboration, *Performance of the ATLAS Trigger System in 2010*, Eur.Phys.J. **C72** (2012) 1849, arXiv: 1110.1530 [hep-ex].

[29] ATLAS Collaboration, *Improved luminosity determination in pp collisions at sqrt(s) = 7 TeV using the ATLAS detector at the LHC*, Eur.Phys.J. **C73**.8 (2013) 2518, arXiv: 1302.4393 [hep-ex].

[30] J. Alwall et al., *MadGraph 5 : Going Beyond*, *JHEP* **06** (2011) 128, arXiv: 1106.0522 [hep-ph].

[31] T. Sjostrand et al., *An Introduction to PYTHIA 8.2*, Comput. Phys. Commun. **191** (2015) 159, arXiv: 1410.3012 [hep-ph].

[32] L. Lonnblad and S. Prestel, *Matching Tree-Level Matrix Elements with Interleaved Showers*, JHEP **03** (2012) 019, arXiv: 1109.4829 [hep-ph].

[33] ATLAS Collaboration, *Summary of ATLAS Pythia 8 tunes*, ATL-PHYS-PUB-2012-003 (2012), URL: http://cdsweb.cern.ch/record/1474107.

[34] R. D. Ball et al., *Parton distributions with LHC data*, Nucl. Phys. **B867** (2013) 244, arXiv: 1207.1303 [hep-ph].

[35] D. J. Lange, *The EvtGen particle decay simulation package*, Nucl. Instrum. Meth. **A462** (2001).

[36] T. Gleisberg et al., *Event generation with SHERPA 1.1*, JHEP **0902** (2009) 007, arXiv: 0811.4622 [hep-ph].

[37] W. Beenakker et al., *Squark and gluino production at hadron colliders*, *Nucl. Phys.* **B 492** (1997) 51, arXiv: hep-ph/9610490.

[38] A. Kulesza and L. Motyka, *Threshold resummation for squark-antisquark and gluino-pair production at the LHC*, *Phys. Rev. Lett.* **102** (2009) 111802, arXiv: 0807.2405 [hep-ph].

[39] A. Kulesza and L. Motyka, *Soft gluon resummation for the production of gluino-gluino and squark-antisquark pairs at the LHC*, *Phys. Rev.* **D 80** (2009) 095004, arXiv: 0905.4749 [hep-ph].

[40] W. Beenakker et al., *Soft-gluon resummation for squark and gluino hadroproduction*, *JHEP* **12** (2009) 041, arXiv: 0909.4418 [hep-ph].

[41] W. Beenakker et al., *Squark and gluino hadroproduction*, *Int. J. Mod. Phys.* **A 26** (2011) 2637, arXiv: 1105.1110 [hep-ph].

[42] M. Krämer et al., *Supersymmetry production cross sections in pp collisions at* $\sqrt{s} = 7$ *TeV* (2012), arXiv: 1206.2892 [hep-ph].

[43] T. Gleisberg and S. Hoche, *Comix, a new matrix element generator*, JHEP **0812** (2008) 039, arXiv: 0808.3674 [hep-ph].

[44] F. Cascioli, P. Maierhofer and S. Pozzorini, *Scattering Amplitudes with Open Loops*, Phys. Rev. Lett. **108** (2012) 111601, arXiv: 1111.5206 [hep-ph].

[45] S. Schumann and F. Krauss, *A Parton shower algorithm based on Catani-Seymour dipole factorisation*, JHEP **0803** (2008) 038, arXiv: 0709.1027 [hep-ph].

[46] S. Hoeche et al., *QCD matrix elements + parton showers: The NLO case*, JHEP **04** (2013) 027, arXiv: 1207.5030 [hep-ph].

[47] S. S. S. Höche F. Krauss and F. Siegert, *QCD matrix elements and truncated showers*, JHEP **0905** (2009) 053, arXiv: 0903.1219 [hep-ph].

[48] H.-L. Lai et al., *New parton distributions for collider physics*, *Phys. Rev.* **D 82** (2010) 074024, arXiv: 1007.2241 [hep-ph].

[49] F. P. R. Gavin Y. Li and S. Quackenbush, *FEWZ 2.0: A code for hadronic Z production at next-to-next-to-leading order*, Comput. Phys. Commun. **182** (2011) 2388, arXiv: 1011.3540 [hep-ph].

[50] S. Alioli et al., *A general framework for implementing NLO calculations in shower Monte Carlo programs: the POWHEG BOX*, JHEP **1006** (2010) 043, arXiv: 1002.2581 [hep-ph].

[51] P. Artoisenet et al., *Automatic spin-entangled decays of heavy resonances in Monte Carlo simulations*, JHEP **1303** (2013) 015, arXiv: 1212.3460 [hep-ph].

[52] T. Sjöstrand, S. Mrenna and P. Skands, *PYTHIA 6.4 Physics and Manual*, JHEP **0605** (2006) 026, arXiv: hep-ph/0603175.

[53] J. Pumplin et al., *New generation of parton distributions with uncertainties from global QCD analysis*, *JHEP* **07** (2002) 012, arXiv: hep-ph/0201195 [hep-ph].

[54] P. Z. Skands, *Tuning Monte Carlo Generators: The Perugia Tunes*, Phys. Rev. **D82** (2010) 074018, arXiv: 1005.3457 [hep-ph].

[55] M. Czakon, P. Fiedler and A. Mitov, *Total Top-Quark Pair-Production Cross Section at Hadron Colliders Through $O(\alpha_S^4)$*, *Phys. Rev. Lett.* **110** (2013) 252004, arXiv: 1303.6254 [hep-ph].

[56] M. Czakon and A. Mitov, *Top++: A Program for the Calculation of the Top-Pair Cross-Section at Hadron Colliders* (2011), arXiv: 1112.5675 [hep-ph].

[57] K. M. A. Lazopoulos T. McElmurry and F. Petriello, *Next-to-leading order QCD corrections to $t\bar{t}Z$ production at the LHC*, *Phys. Lett.* **B 666** (2008) 62, arXiv: 0804.2220 [hep-ph].

[58] J. M. Campbell and R. K. Ellis, *$t\bar{t}W^{\pm}$ production and decay at NLO*, *JHEP* **07** (2012) 052, arXiv: 1204.5678 [hep-ph].

[59] ATLAS Collaboration, *The ATLAS Simulation Infrastructure*, *Eur. Phys. J.* **C 70** (2010) 823, arXiv: 1005.4568 [physics.ins-det].

[60] S. Agostinelli et al., *GEANT4: A simulation toolkit*, *Nucl. Instrum. Meth.* **A 506** (2003) 250.

[61] ATLAS Collaboration, *The simulation principle and performance of the ATLAS fast calorimeter simulation FastCaloSim*, ATL-PHYS-PUB-2010-013 (2010), URL: http://cds.cern.ch/record/1300517.

[62] M. Cacciari, G. P. Salam and G. Soyez, *The anti-k_t jet clustering algorithm*, *JHEP* **04** (2008) 063, arXiv: 0802.1189 [hep-ph].

[63] M. Cacciari and G. P. Salam, *Dispelling the N^3 myth for the k_t jet-finder*, *Phys. Lett.* **B 641** (2006) 57, arXiv: hep-ph/0512210.

[64] W. Lampl et al., *Calorimeter Clustering Algorithms: Description and Performance*, ATL-LARG-PUB-2008-002 (2008), URL: http://cdsweb.cern.ch/record/1099735.

[65] ATLAS Collaboration, *Jet energy measurement with the ATLAS detector in proton-proton collisions at $\sqrt{s} = 7$ TeV*, *Eur. Phys. J.* **C 73** (2013) 2304, arXiv: 1112.6426 [hep-ex].

[66] M. Cacciari and G. P. Salam, *Pileup subtraction using jet areas*, *Phys. Lett.* **B 659** (2008) 119, arXiv: 0707.1378 [hep-ph].

[67] ATLAS Collaboration, *Performance of pile-up mitigation techniques for jets in pp collisions at $\sqrt{s} = 8$ TeV using the ATLAS detector* (2015), arXiv: 1510.03823 [hep-ex].

[68] ATLAS Collaboration, *Jet Calibration and Systematic Uncertainties for Jets Reconstructed in the ATLAS Detector at $\sqrt{s} = 13$ TeV*, ATL-PHYS-PUB-2015-015 (2015), URL: http://cdsweb.cern.ch/record/2037613.

[69] ATLAS Collaboration, *Expected performance of the ATLAS b-tagging algorithms in Run-2*, ATL-PHYS-PUB-2015-022 (2015), URL: http://cdsweb.cern.ch/record/2037697.

[70] ATLAS Collaboration,
Commissioning of the ATLAS b-tagging algorithms using $t\bar{t}$ events in early Run-2 data,
ATL-PHYS-PUB-2015-039 (2015), URL: http://cdsweb.cern.ch/record/2047871.

[71] ATLAS Collaboration,
Selection of jets produced in proton-proton collisions with the ATLAS detector using 2015 data,
ATLAS-CONF-2015-029 (2015), URL: http://cdsweb.cern.ch/record/2037702.

[72] ATLAS Collaboration,
Electron identification measurements in ATLAS using $\sqrt{s}$ = 13 TeV data with 50 ns bunch spacing,
ATL-PHYS-PUB-2015-041 (2015), URL: http://cdsweb.cern.ch/record/2048202.

[73] ATLAS Collaboration, *Muon reconstruction performance in early Run II*,
ATL-PHYS-PUB-2015-037 (2015), URL: http://cdsweb.cern.ch/record/2047831.

[74] ATLAS Collaboration, *Expected performance of missing transverse momentum reconstruction for the ATLAS detector at $\sqrt{s}$ = 13 TeV*, ATL-PHYS-PUB-2015-023 (2015),
URL: http://cdsweb.cern.ch/record/2037700.

[75] ATLAS Collaboration, *Measurements of the Photon Identification Efficiency with the ATLAS Detector using 4.9 fb^{-1} of pp Collision Data Collected in 2011*, ATLAS-CONF-2012-123 (2012),
URL: http://cdsweb.cern.ch/record/1473426.

[76] M. Baak et al., *HistFitter software framework for statistical data analysis*,
Eur. Phys. J. **C 75**.4 (2015) 153, arXiv: 1410.1280 [hep-ex].

[77] A. L. Read, *Presentation of Search Results: The CL(s) Technique*, J. Phys. G **28** (2002) 2693.

[78] C. Chen, *New approach to identifying boosted hadronically decaying particles using jet substructure in its center-of-mass frame*, Phys.Rev. **D85** (2012) 034007,
arXiv: 1112.2567 [hep-ph].

[79] ATLAS Collaboration, *Single hadron response measurement and calorimeter jet energy scale uncertainty with the ATLAS detector at the LHC*, *Eur. Phys. J.* **C 73** (2013) 2305,
arXiv: 1203.1302 [hep-ex].

[80] ATLAS Collaboration, *Jet energy resolution in proton-proton collisions at $\sqrt{s}$ = 7 TeV recorded in 2010 with the ATLAS detector*, *Eur. Phys. J.* **C 73** (2013) 2306, arXiv: 1210.6210 [hep-ex].

[81] S. Frixione and B. R. Webber, *Matching NLO QCD computations and parton shower simulations*, *JHEP* **06** (2002) 029, arXiv: hep-ph/0204244.